DOCUMENT

Analysis of the NIRSpec Demonstration Model Measurements at Ambient

James Webb Space Telescope

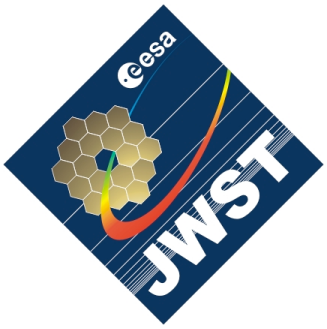

prepared by	ESA NIRSpec Instrument Calibration Team
approved by	Peter Jakobsen
reference	ESA-JWST-RP-11883
issue	1
revision	0
date of issue	04 December 2008

European Space Agency
Agence spatiale européenne

ESTEC
Keplerlaan 1 - NL 2201 AZ Noordwijk ZH - The Netherlands
Tel (31) 71 565 4920 - Fax (31) 71 565 8371 - http://sci.esa.int/jwst

1 Introduction

The scope of this document is to present our analyis of the optical measurements made on the NIRSpec Demonstration Model (DM) under ambient conditions in October 2008 at Astrium. The results presented here were derived independently. A separate report on these measurements will also be prepared by Astrium.

The NIRSpec DM is intended to work only in imaging mode and samples only the first – but most sophisticated – element of the optical chain of the instrument; namely the Fore Optics, which are designed to re-image the curved focal surface of the JWST telescope onto the flat surface of the Micro Shutter Array (MSA) in a telecentric manner. The NIRSpec DM consists of the Qualification Models of the NIRSpec Fore Optics and the Refocussing Mechanism Assembly (RMA). For the tests described here, a pupil stop located at the position of the filter wheel defined the f-ratio of the output beam. This stop also carried a 10 mm CaF_2 filter that was tilted by 5.3 degrees in the spatial direction in the manner prescribed for the Flight Instrument. For the ambient measurements, a dedicated CCD detector on an x-y-z translation table was located at the output focal plane in place of the Micro-Shutter Array (MSA). For the future tests to be carried out at cryogenic conditions, the CCD detector and its translation table will be replaced by the Engineering Model of the NIRSpec HdCdTe near-infrared detector array and the pupil stop will be replaced by the Structural Thermal Model of the NIRSpec Filter Wheel Assembly (FWA). The FWA also contains a pupil stop and a 10 mm thick CaF_2 filter, albeit with the latter in a non-tilted configuration (i.e. mounted orthogonal to the chief ray).

2 Measurements and Data

In order to map the distortion of the Fore Optics at ambient, a grid of 10×10 fibers with accurately known positions in the OTE focal plane was imaged through the NIRSpec DM onto the MSA plane. Measurements were carried out with the fiber array (called the Illumination Distortion Grid, IDG) located at three positions along the optical axis. For each fiber array position, measurements were made at nine settings of the RMA, covering the entire ± 3 mm travel range.

All data was taken with a CCD detector, and at a wavelength of ~ 540 nm. The CCD has 5360×4128 pixels with a size of $9\,\mu\text{m} \times 9\,\mu\text{m}$. In order to cover the full MSA focal plane, the CCD was moved by means of an x-y-z-table. Twelve overlapping CCD positions were used in a 4×3 grid, with the longer CCD edge parallel to the MSA y-coordinate (see Fig. 1). At each of these 12 positions, three "dithered" exposures were taken with very small offsets in CCD position ($\sim 100\,\mu$m in x and y). The x-axis of the MSA plane corresponds to the dispersion direction in NIRSpec, whereas the y-axis corresponds to the cross-dispersion direction.

Due to the 4×3 pattern with 3 sub-exposures, each fiber was imaged at least three times by the CCD. Fibers towards the center of the MSA field were covered more often, up to 18 times, because of the overlap between different CCD images.

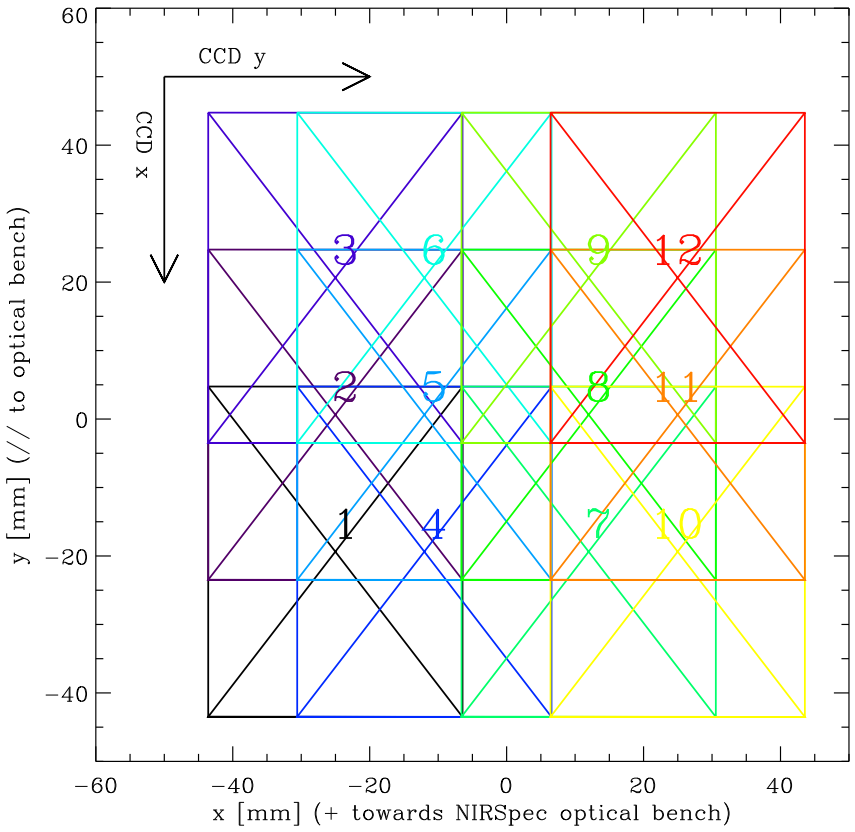

Figure 1: The coverage of the 12 CCD positions in the MSA. The x-direction corresponds to the dispersion direction.

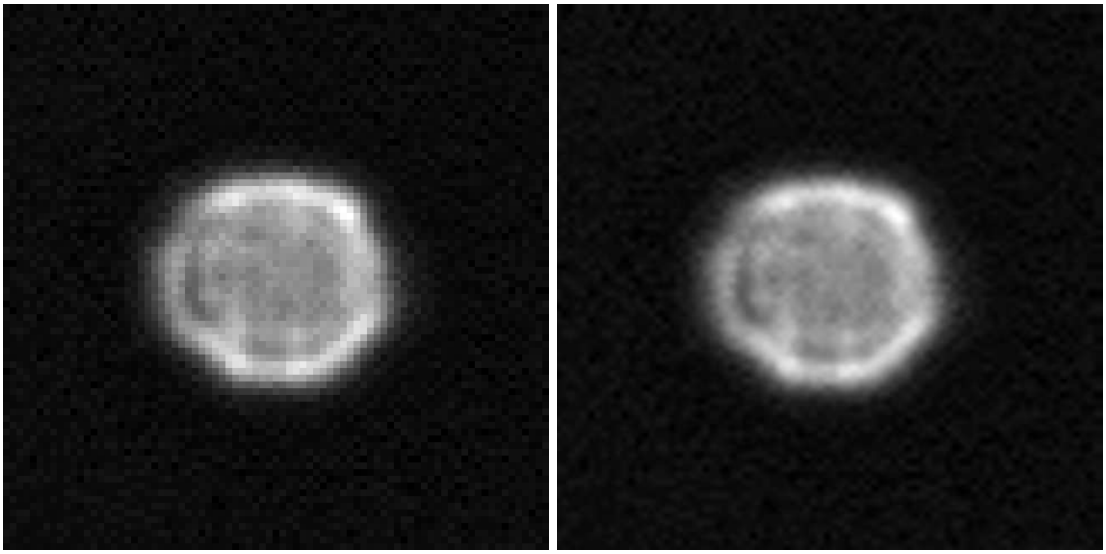

Figure 2: Typical out of focus image of a fiber with the original pixel scale (left) and six-times cubic oversampling (right).

2.1 Centering the fiber images

For RMA settings away from the optimal focus position, the defocused images of the fibers in the MSA plane get quite large and show a complex morphology (see Fig. 2). Therefore, standard centroiding can be inaccurate, and we instead used ellipse fitting to derive the center and width of the light distribution.

The ellipse fitting was done in two steps. First, the coarse positions of the fiber images on the CCD were found by selecting all pixels above a given threshold, typically 20 times the standard deviation of the (background-subtracted) image. Then, the CCD regions around the fiber images were extracted and resampled to six times the original resolution. The ellipse was then fitted to a region of interest that was defined by all pixels with a flux greater than 30% of the maximum flux in the particular fiber image. This threshold of 30% is an arbitrary value, chosen because it yielded good results also for the complex shapes, but the exact value is uncritical.

2.2 From CCD to physical coordinates

In order to transform the measured fiber positions from CCD coordinates (pixels) to physical coordinates in the MSA plane, we use the transformation given by Astrium (Xavier Gnata):

$$\begin{aligned} x_{\mathrm{FRF}} &= -9.39516411417246 \times 10^{-7} \times x_{\mathrm{CCD}} + 0.0089995993252693 \times y_{\mathrm{CCD}} \\ &\quad -18.592 + \mathrm{M1FRFX} \\ y_{\mathrm{FRF}} &= -0.0089995993252693 \times x_{\mathrm{CCD}} - 6.46322496819795 \times 10^{-6} \times y_{\mathrm{CCD}} \\ &\quad +24.7584 + \mathrm{M1FRFY} \end{aligned}$$

where $x_{\rm FRF}, y_{\rm FRF}$ are the physical coordinates in the MSA plane in mm, $x_{\rm CCD}, y_{\rm CCD}$ the centers of the fiber images in pixels, and M1FRFX, M1FRFY the reference position of the CCD.

This transformation gives good, but not perfect results when combining the different CCD positions (see Fig. 3). For images of fibers that were only taken at one CCD position (i.e. at the corners), the spread between the three dithered measurements is below 1 μm, indicating good repeatability of the ellipse fitting. Fiber images that were taken with significant CCD movements in between show a larger scatter.

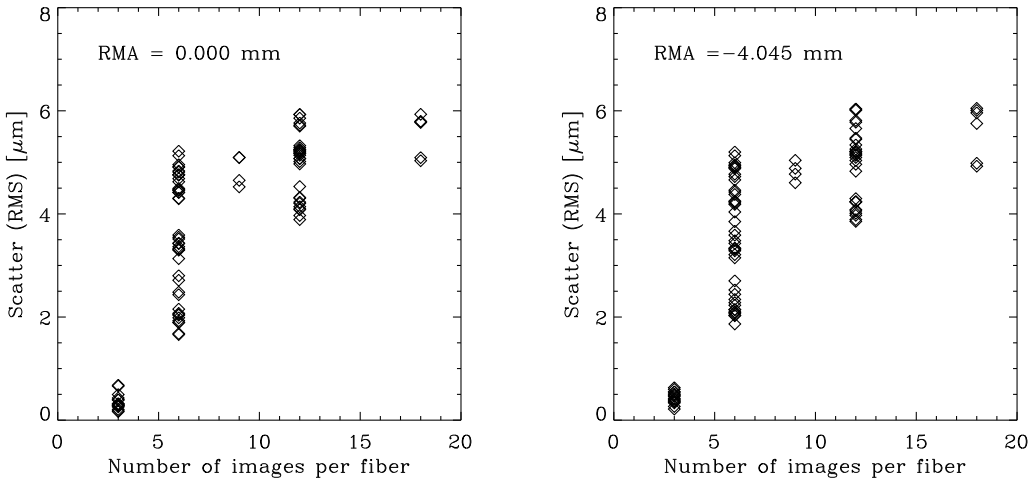

Figure 3: The scatter of the measured ellipse centers in MSA coordinates as a function of the number of times a given fiber image was observed.

3 Results

3.1 Focus

3.1.1 RMA sweep

The width of the semimajor and semiminor axes of the fitted ellipses are shown in Figures 4 to 6 for each position of the fiber array. The plots show the focus curves for the four corners of the field, a fiber near the center, and the average over all 100 fibers. The defocus was computed using the nominal RMA position as reference and taking into account the pentaprism design of the RMA focus mechanism. Due to this, a RMA movement of x mm leads to a defocus in the MSA plane of $\Delta f = \sqrt{2} \times x$ mm. Straight lines were fitted to the data excluding points with a width smaller than 30 μm, yielding a good fit and consistent estimates for the best focus position. The v-shape of the focus curves merely reflects the f/12.5 focal ratio of the Fore Optics output beam. When going out of the best focus position, the beam at the MSA plane is sliced further and further

away from its smallest extent, yielding a linear dependence of fiber image half width with defocus with a slope of $|s| = \frac{1}{2 \times f/12.5} = 0.04$, in good agreement with the slopes of the linear fits.

The estimates for best focus for the three different positions of the fiber array inferred from Figures 4, 5 and 6 can be compared to the nominally expected ones, taking into account the net magnification factor of the Fore Optics (0.616 by design). A change in IDG object position of ΔIDG will lead to a change in image focus at the MSA of $0.616^2 \times \Delta$IDG. The determined best focus values are compared to the ones calculated from ΔIDG in Table 1. The agreement is quite good.

Table 1: Comparison of measured and estimated focus positions.

ΔIDG [mm]	$0.616^2 \times \Delta$IDG	Δ(measured defocus) [mm]
$+3.10$	$+1.176$	$+1.138 \pm 0.104$
-1.33	-0.505	-0.518 ± 0.089

3.1.2 Fiber image size distribution

Fig. 7 shows the distribution of fiber locations in the MSA plane and their derived sizes for six different RMA settings, going from out of focus (RMA = -2.860 mm, defocus = -4.045 mm) to best (nominal) focus at 0.0 mm and out again (RMA = $+3.140$ mm, defocus = $+4.441$ mm). The homogeneous distribution of measured fiber image widths indicates that the best focus is achieved simultaneously over the entire FOV, i.e. that the NIRSpec Fore Optics indeed produces a flat image at the MSA focal plane - and that the CCD is well aligned with this image.

3.1.3 CCD sweep

In order to sample the focus curve around the nominal focus position of the RMA better, the CCD was moved in the z-direction out of the MSA plane. For this measurement only the central part of the MSA plane was imaged and no movement in the x or y-directions took place. Also it was done with the IDG at nominal position only.

The result is shown in Fig. 8, indicating that the best focus is in fact very close to the nominal one. When comparing Fig. 8 with Fig. 4, one has to consider the different scale on the y-axis. The observed widths reasonably follow a parabola around best focus.

3.2 Telecentricity

The NIRSpec Fore Optics are designed to be telecentric, such that the f/12.5 output beam of the system is perpendicular to the MSA focal plane for all field positions. Moving the RMA should therefore ideally not lead to a displacement of the fiber images nor to a change in magnification in the MSA focal plane, but only result in a defocus of the fiber images.

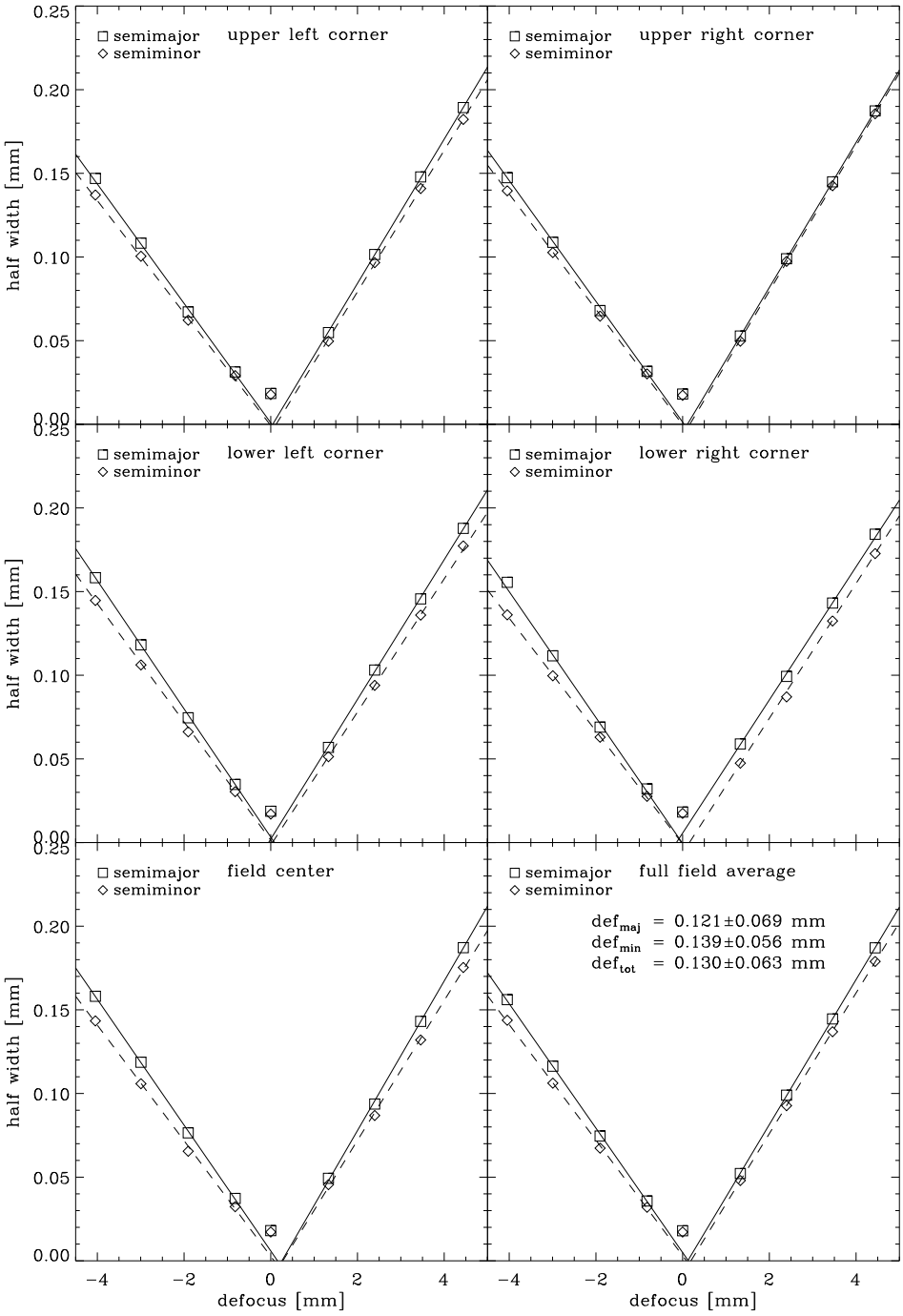

Figure 4: The focus curves for five different fiber images obtained with the fiber array at its nominal position (IDG = 0.0 mm).

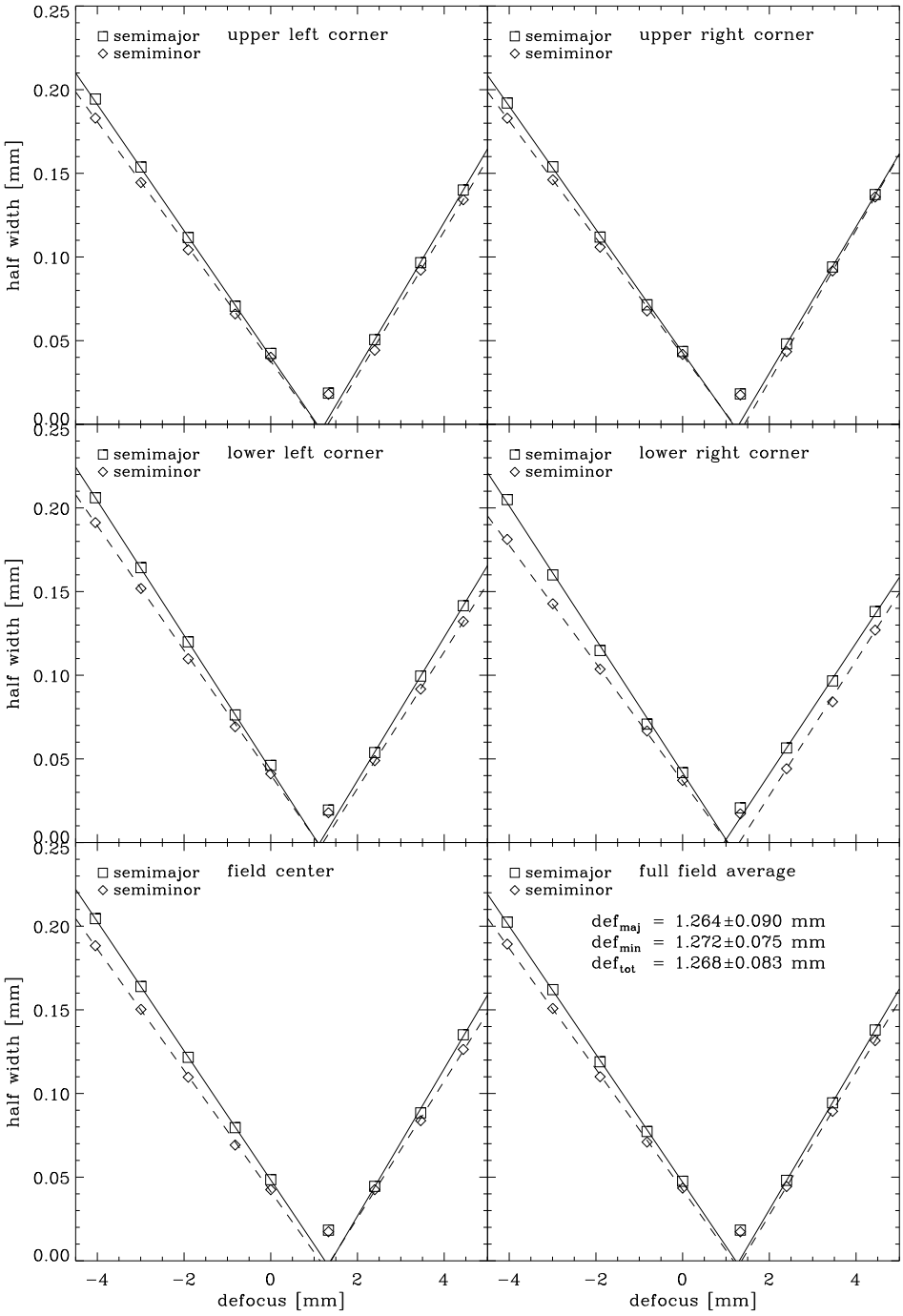

Figure 5: The focus curves for five different fiber images obtained with the fiber array moved 3.1 mm from its nominal position towards the pickoff mirror (IDG = +3.1 mm).

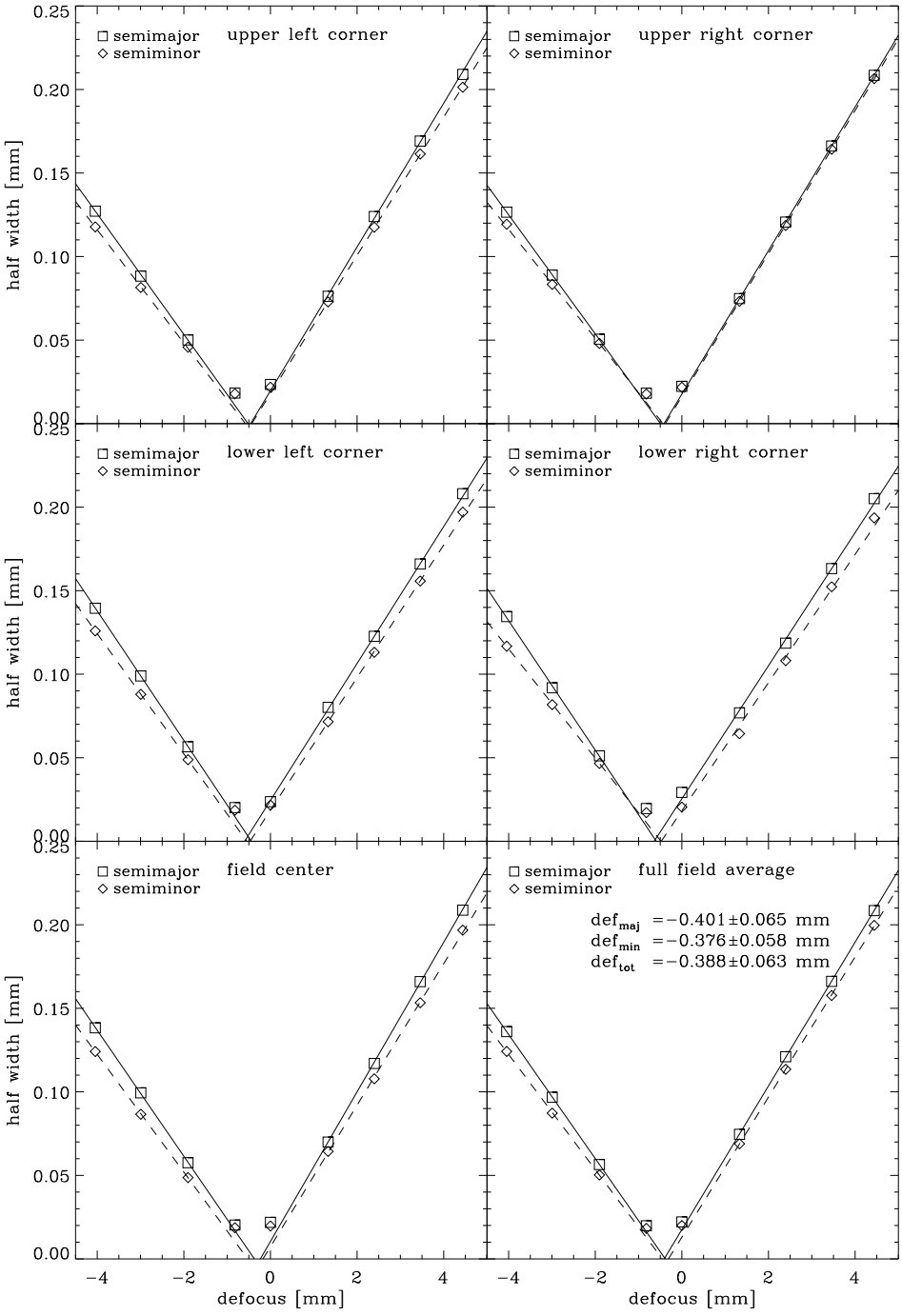

Figure 6: The focus curves for five different fiber images obtained with the fiber array moved 1.33 mm from its nominal position away from the pickoff mirror (IDG = -1.33 mm).

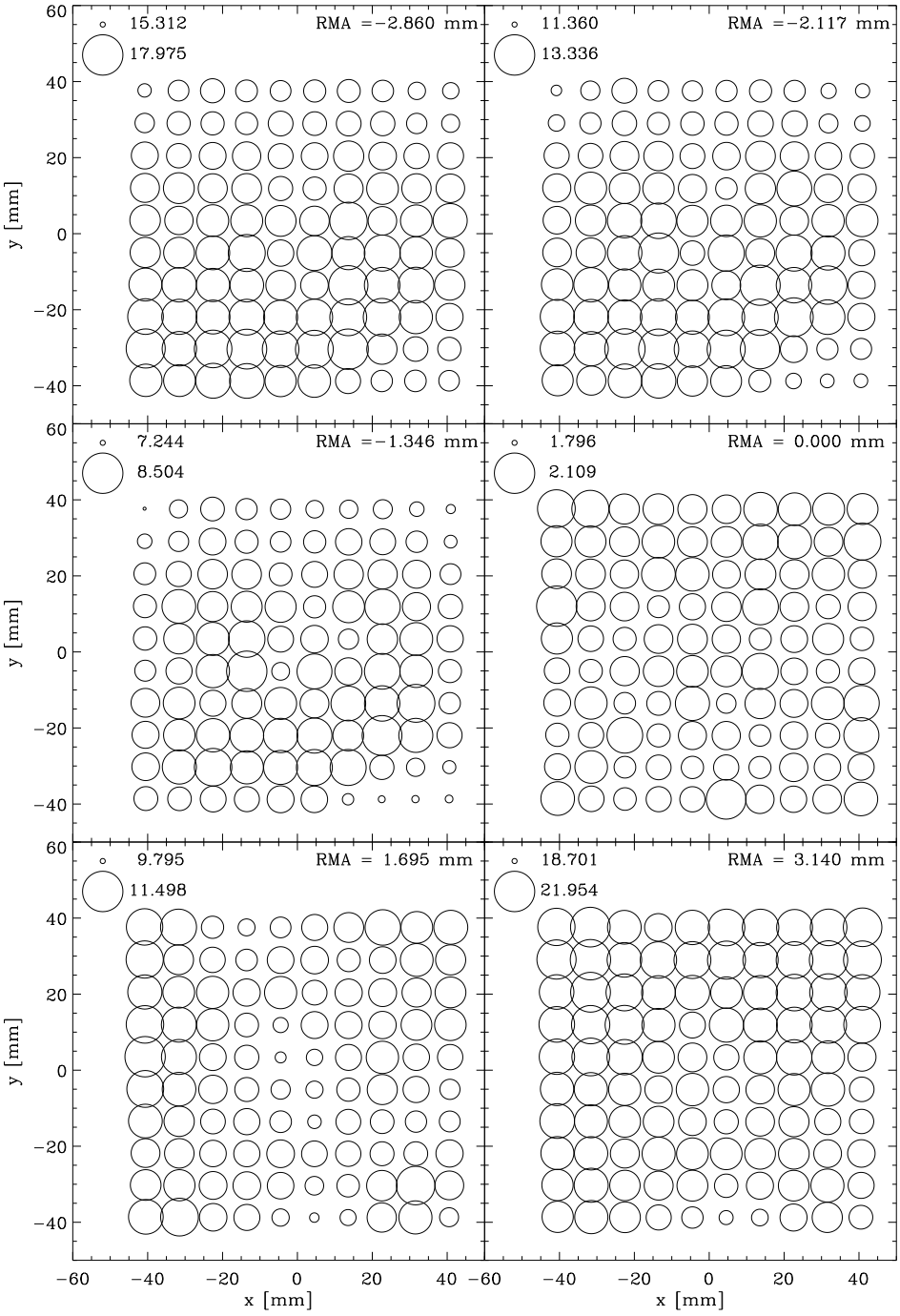

Figure 7: The distribution of fiber image widths in the MSA plane for different RMA positions. Please note the different size scales denoted in the upper left of each panel. In each case the smallest and largest circle in the scale correspond to a range of ±8% around the mean widths.

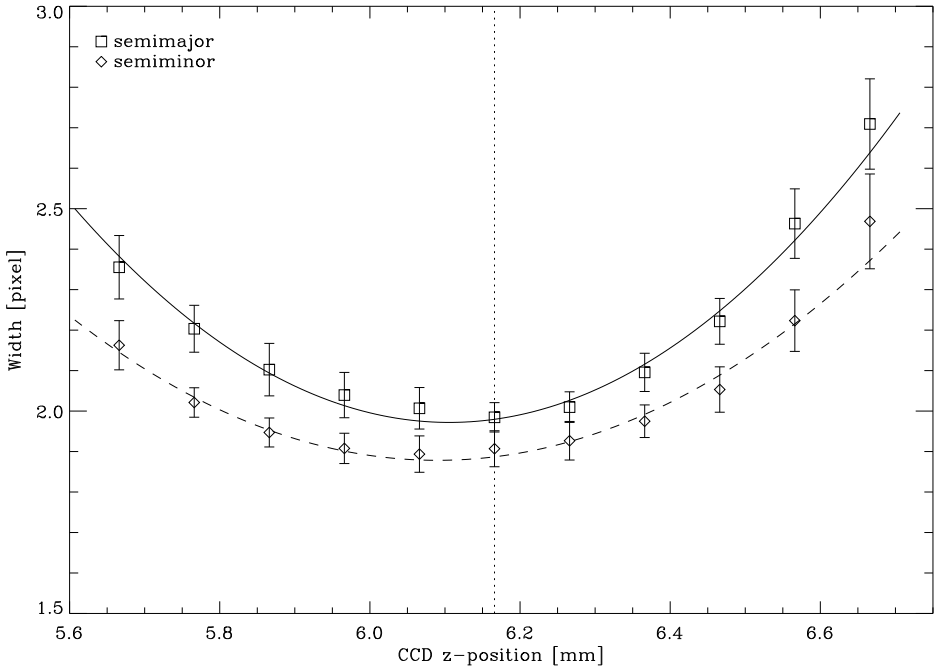

Figure 8: The average semimajor and semiminor width of the 24 fiber images in the field of view of the CCD for different CCD positions in z. The error bars denote the standard deviation of these widths. The solid and dashed lines correspond to a parabolic fit, the vertical dotted line shows the nominal position of the CCD in the MSA plane.

Using the data for the best focus RMA position with the fiber grid at its nominal position as reference, Fig. 9 shows the computed shifts, relative scale changes, and rotation when moving the RMA.

A small, but systematic, image shift together with an accompanying slight change in image scale are, in fact, detected when moving the RMA. The image shift is primarily in the x (dispersion) direction, and amounts to approximately $\Delta x \simeq \pm 18\,\mu$m over the full ± 3 mm stroke of the RMA. This shift is presumably caused by an unintended gradual tilting of the RMA roof mirror assembly in the dispersion direction perpendicular to the optical bench as it moves along its linear displacement mechanism.

The observed change in magnification with RMA position is detected in both x and y at the level of $\Delta m/m \simeq \pm 0.02\%$ over the full RMA stroke. Its cause is less clear, but it could conceivably arise from residual power in the moving RMA roof mirrors. The measured scale change is equivalent to a maximum total image displacement of $\Delta d \sim \pm 14\,\mu$m at the extreme corner of the MSA plane.

While neither of these RMA-induced effects is desirable, they are small enough to not cause serious concern. In particular, the corresponding contributions to the initial uncertainty in the knowledge of the in-orbit location of the NIRSpec field of view and its plate scale are completely overwhelmed by the much larger uncertainties in the bulk NIRSpec/ISIM/OTE metrology and the lack of knowledge of the final focal length and focus location of the OTE once it has been phased and optimized in orbit.

Since the RMA is anticipated to be operated only once after launch, and then kept locked at its optimal position, the RMA-induced image shift and magnification change described above will effectively act as additional, but stable, contributions to the total sky-to-MSA transformation that will be included in the in-orbit calibration. Assuming that the location of the OTE focus will deviate from its nominal position w.r.t. NIRSpec by at most $\Delta f_{OTE} = \pm 2$ mm, this corresponds to an initial required compensatory RMA movement of only $\Delta\mathrm{RMA} = \pm 0.54$ mm, i.e. less than one fifth of the full RMA stroke. The RMA-induced image shift and magnification change over this span in RMA position are: $\Delta x = \pm 3.2\,\mu$m and $\Delta m = \pm 2 \times 10^{-4}$. Once the initial OTE focus position has been established, the JWST operational plan calls for the OTE focus to be held in position to a much higher accuracy of $\Delta f_{OTE} = \pm 0.17$ mm, equivalent to 1.5% of the full RMA stroke.

Assuming that the above deviations from a perfectly telecentric system do not worsen under cryo conditions, we tentatively conclude that the NIRSpec DM appears to be more than sufficiently telecentric for NIRSpec's needs.

3.3 Geometric Transformations - Magnification and Zero Point

To measure the transformation between the OTE/fiber array plane and the MSA plane, the measured fiber positions at the OTE focus (provided by Astrium through Xavier Gnata) were compared with the measured positions of the fiber images at the MSA plane using the 'geomap' task in IRAF. This routine first calculates the best fit linear transformation (zero point, scale in x and y and rotation) between the input and output

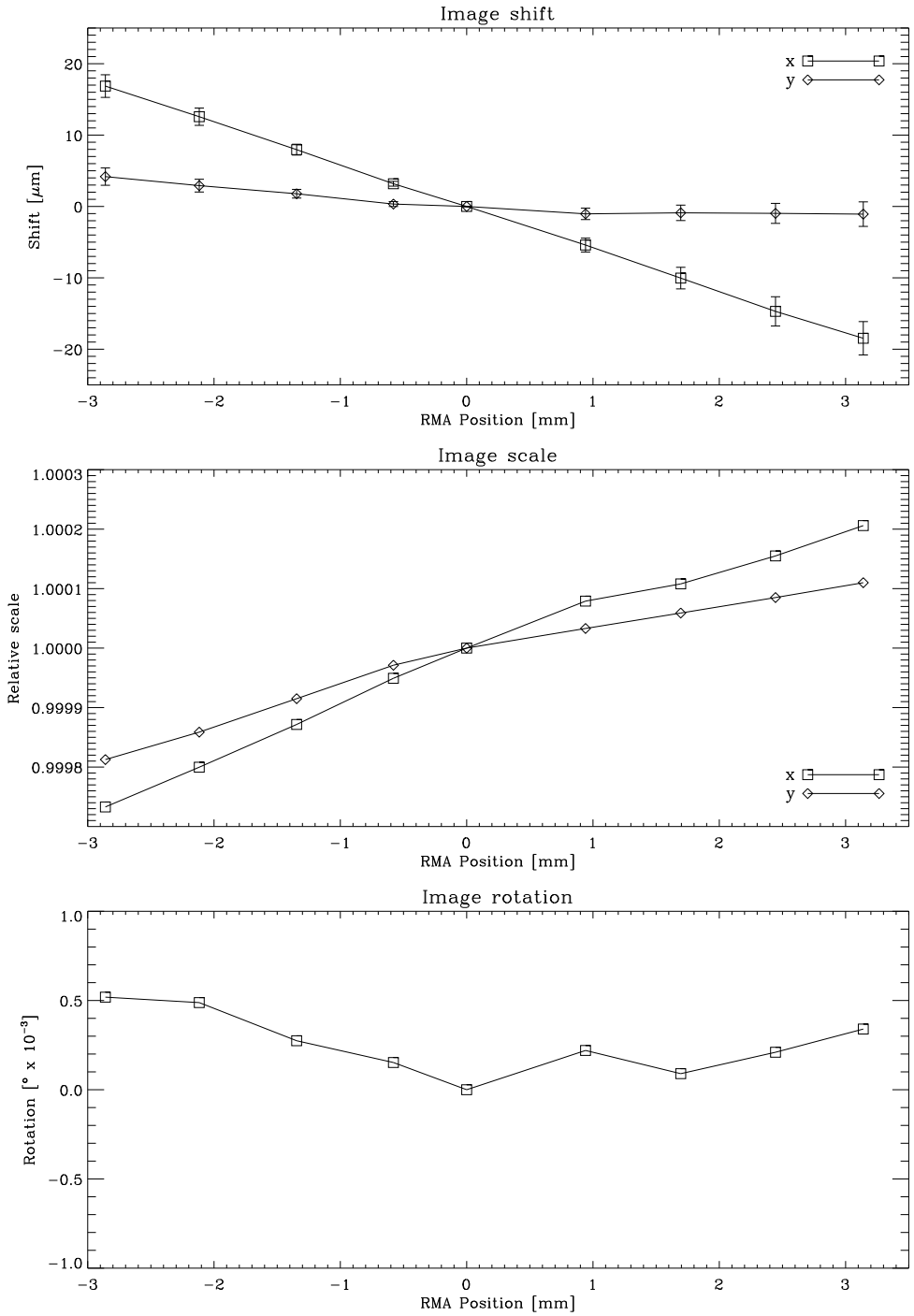

Figure 9: The relative image shift, magnification, and rotation when moving the RMA. Data has been taken with the fiber array at its nominal position (IDG = 0.0 mm).

data, and then calculates a distortion map by fitting two-dimensional polynomials to the residuals in each axis from the best fit linear solution.

The results for the best fit linear components are summarized in Table 2 below. Shift is given in $x_{\rm MSA}$, $y_{\rm MSA}$, the magnification is in $x_{\rm MSA}/x_{\rm IDG}$, $y_{\rm MSA}/y_{\rm IDG}$, respectively. All data were computed for the RMA closest to best focus for any given IDG position (taken from Figures 4 to 6).

Table 2: The zero point (shift), magnification, and rotation between the OTE and MSA plane for three different positions of the fiber array (IDG).

	shift [mm]		magnification		rotation [°]
IDG [mm]	x	y	x	y	
0.0	0.035	-0.705	0.61408	0.60506	0.056
+3.1	0.038	-0.728	0.61352	0.60448	0.055
-1.33	0.037	-0.713	0.61431	0.60531	0.056

The as-built magnifications of the Fore Optics Qualification Model measured at ambient by SAGEM are $m_x = 0.6137 \pm 0.0003$ and $m_y = 0.6058 \pm 0.0003$ (NIRS-SAG-TR-0439), in good agreement with our measured values for the nominal IDG position. When changing the IDG position by ΔIDG the expected change in magnification is

$$\Delta m_{x,y} = \frac{m_{x,y}2}{f}\Delta\mathrm{IDG}, \tag{1}$$

where $m_{x,y}$ are the nominal magnifications in x and y and $f = -2143\,$mm the nominal focal length of the Fore Optics. For $\Delta\mathrm{IDG} = +3.1\,$mm and $\Delta\mathrm{IDG} = -1.33\,$mm the expected shifts are $\Delta m_x = -0.00055$, $\Delta m_y = -0.00053$ and $\Delta m_x = 0.00023$, $\Delta m_y = 0.00023$, in excellent agreement with the measured magnification changes seen in Table 2.

3.4 Geometric Transformations - Distortion

The linear transformations given in Table 2 are not expected to provide a perfect translation from IDG to MSA coordinates, because the Fore Optics are known to suffer from optical distortion. This distortion can be well described with polynomial terms, as shown in Fig. 10. For a 4th order polynomial the residuals of the transformation become $\lesssim 1.5\,\mu$m, which is likely the limit set by the finite centering accuracy of the fiber images and knowledge of the absolute fiber locations on the IDG.

The measured distortion maps of the MSA plane are shown in Figures 11 to 13. These maps give the non-linear part of the transformation (i.e. the residuals as a function of position in the MSA plane once the best fit linear transformation has been subtracted), fitted using 4th order polynomials.

The first question to ask is whether these measured distortion maps bear any resemblance to the anticipated ones inferred from ZEMAX ray tracing of the NIRSpec optical

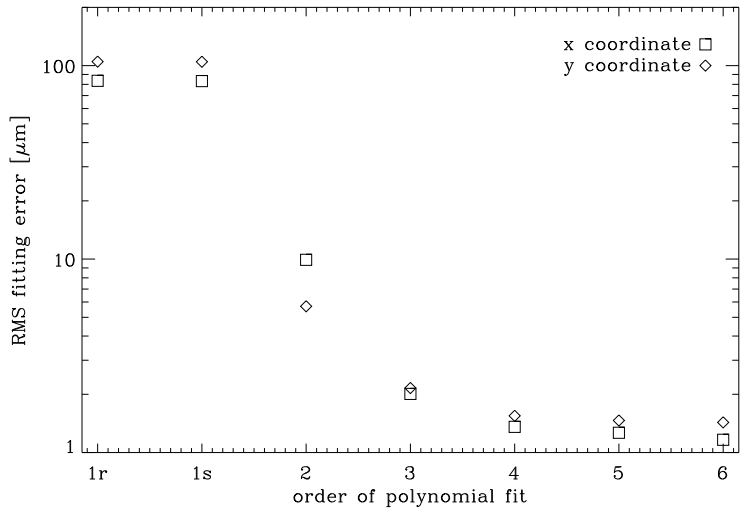

Figure 10: The rms residuals of the fit of the geometric transformation from OTE to MSA plane using the position of the 100 fibers and fiber images. The x-axis gives the order of the polynomial component (the total power in x and y is equal to order). The '1r' denotes a linear transformation with common rotation, '1s' a linear transformation with shear. It is seen that adding non-linear components to the transformation improves the fit significantly up to orders 4-5.

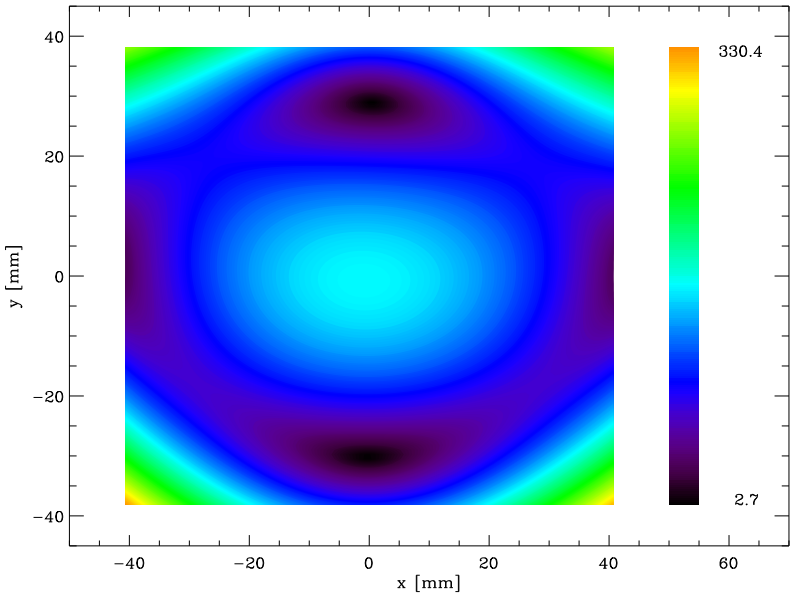

Figure 11: Map of the measured total distortion in the MSA plane fitted with 4th order polynomials. The color bar to the right denotes the magnitude of the distortion in μm.

models. To address this question, we applied the same two step polynomial fitting procedure to the 10×10 IDG fiber positions and their corresponding image locations in the MSA focal plane predicted by the (warm) ZEMAX model of the NIRSpec DM with the IDG located at its nominal position. The ZEMAX predictions were provided by Alexandre Teilhet and include the effect of the tilted CaF_2 filter.

The resulting best fit linear magnifications of the ZEMAX predictions are $m_x = 0.6152$ and $m_y = 0.6063$, in reasonable agreement with the design values of $m_x = 0.616$ and $m_y = 0.604$. The resulting predicted distortion maps with the linear terms subtracted are indeed in close agreement with the measured ones shown in Figures 11 to 13. Figure 14 shows the difference between the measured and expected total distortion maps. The rms residual calculated over the full MSA FOV is 4.1 μm. The peak residual of 32 μm is only reached in one extreme corner of the field.

We conclude that once the differences in zero point and magnification between the designed and as-built Fore Optics QM are accounted for, the measured transformation between OTE and MSA focal planes indeed appears to agree with the predicted one to better than one part in 10^3 over the entire instrument field of view.

It is also of interest is to explore how the measured distortion changes with input IDG position and corresponding best focus RMA position.

Figures 15 and 16 show the differences between the total distortion maps measured at the nominal IDG setting and at the best focus RMA positions for the two offset IDG settings listed in Table 2. The rms residuals in the two cases are 0.15 μm and 0.13 μm.

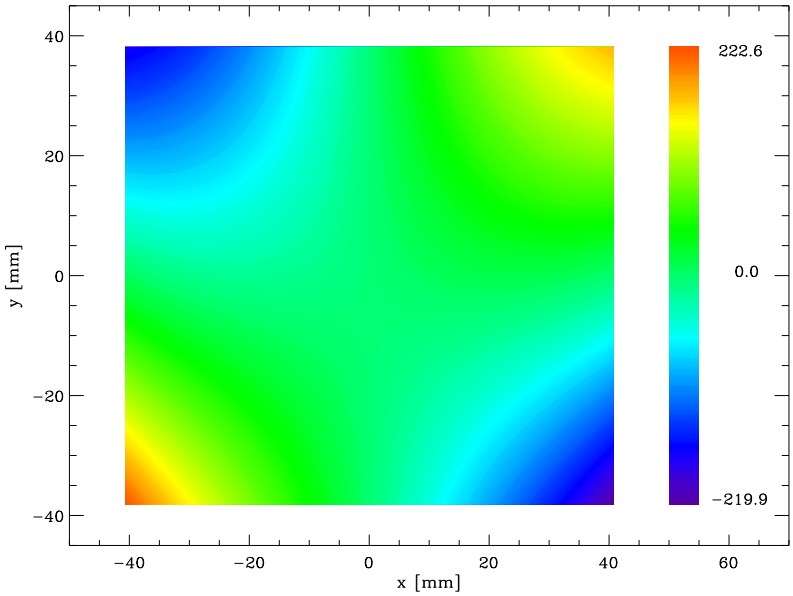

Figure 12: Map of the measured distortion in x fitted with 4th order polynomials. The color bar to the right denotes the difference in μm.

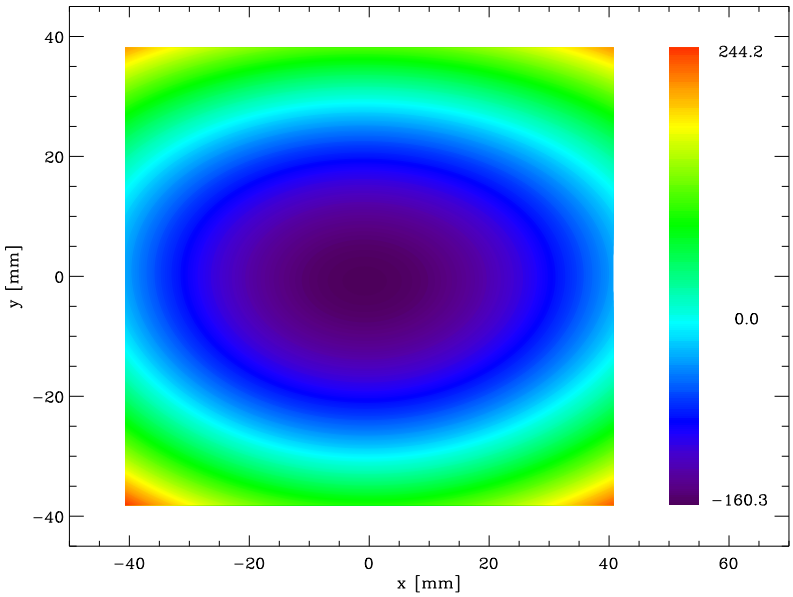

Figure 13: Map of the measured distortion in y fitted with 4th order polynomials. The color bar to the right denotes the difference in μm.

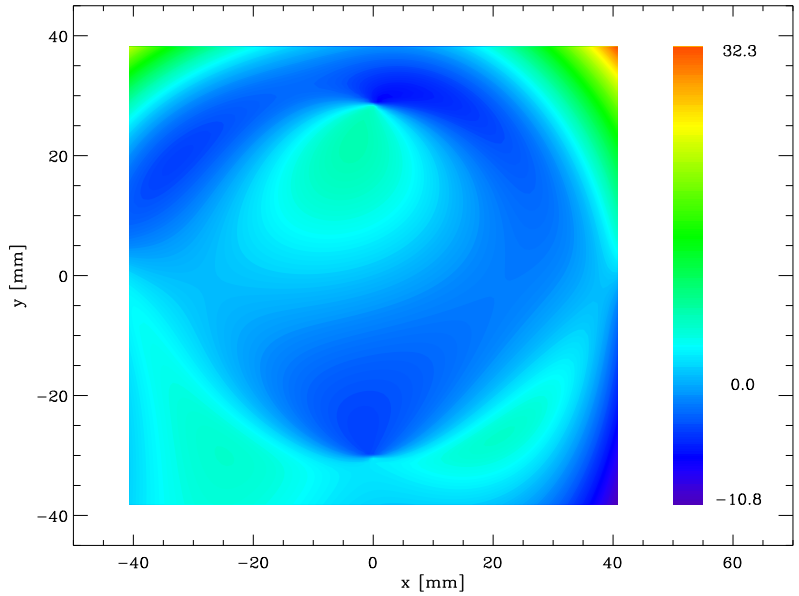

Figure 14: Map of the difference between the measured total distortion and that predicted by the ZEMAX model. The color bar to the right denotes the difference in μm.

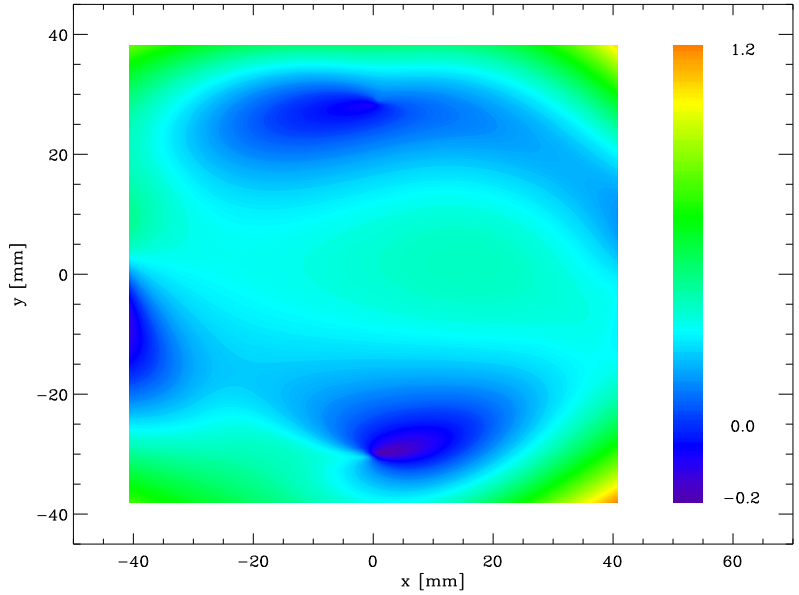

Figure 15: Map of the difference of the total distortion in the MSA plane for the IDG at +3.1 mm compared to its nominal position. The color bar to the right denotes the difference in μm.

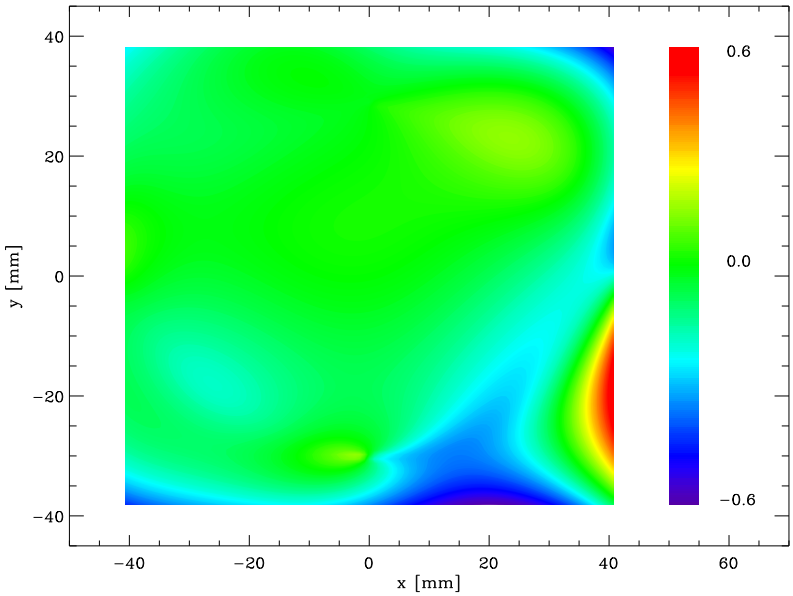

Figure 16: Map of the difference of the total distortion in the MSA plane for the IDG at -1.33 mm compared to its nominal position. The color bar to the right denotes the difference in μm.

It is worth emphasizing that the distortion maps produced by the 'geomap' task refer to the residuals w.r.t. the best fit linear solution. The fact that the distortion maps corresponding to the three cases listed in Table 2 seem to be nearly identical therefore suggests that the underlying distortion pattern of the Fore Optics has simply scaled with the change in output image magnification between the three IDG settings.

This tentative finding is very encouraging from an operational perspective, in that it suggests that it may be feasible to operate with a single "master" distortion map that can be measured pre-launch during the NIRSpec ground calibration campaign and then applied in flight once the center of the NIRSpec field of view and final image plate scales provided by the OTE have been determined in orbit. If feasible, this approach could potentially simplify the on-orbit commissioning of NIRSpec considerably.

3.5 Summary

We have performed a first analysis of the test data taken with the NIRSpec Demonstration Model under ambient conditions in October 2008 at Astrium. Our analysis has uncovered no major surprises, and confirms that the NIRSpec Demonstration Model behaves much as anticipated.

The focus curves obtained by moving the RMA for a fixed IDG position have the anticipated triangular shape consistent with the f/12.5 output beam of the NIRSpec Fore Optics, and show no obvious systematic trends with field position, thereby confirming

that the Fore Optics produces a flat focal plane that appears to have been well aligned with the test CCD detector. Although a slight shift in bulk image location and magnification is detected with RMA movement, these measured deviations from a perfect telecentric system are not of a magnitude that gives cause for serious concern at this point.

The measured image magnifications inferred from the Astrium tests are consistent with the as-built values for the Fore Optics Qualification Model reported by SAGEM. Once the linear scale and zero point differences between the designed and as-built optics are accounted for, the observed residual higher distortion maps agree with the ZEMAX predictions to better than one part in 10^3 over the entire NIRSpec field of view.

The measured shifts in best focus location and net image magnification resulting from a displacement of the input fiber source grid are also entirely consistent with expectations. Moreover, when changes in image magnification are taken into account, the residual higher order distortion appears to be remarkably robust to changes in best focus position, suggesting that the non-linear distortion pattern to a first approximation merely scales with the magnification.

This scaling hypothesis will obviously need to be revisited once the results of the DM cryo tests become available.